Inorganic Chemistry

Article

pubs.acs.org/IC

Evaluating the Identity and Diiron Core Transformations of a (μ-Oxo)diiron(III) Complex Supported by Electron-Rich Tris(pyridyl-2-methyl)amine Ligands

Loi H. Do,[†] Genqiang Xue,[‡] Lawrence Que, Jr.,*[,‡] and Stephen J. Lippard*[,†]

[†]Department of Chemistry, Massachusetts Institute of Technology, Cambridge, Massachusetts 02139, United States

[‡]Department of Chemistry and Center for Metals in Biocatalysis, University of Minnesota, Minneapolis, Minnesota 55455, United States

Supporting Information

ABSTRACT: The composition of a (μ-oxo)diiron(III) complex coordinated by tris[(3,5-dimethyl-4-methoxy)pyridyl-2-methyl]amine (R_3TPA) ligands was investigated. Characterization using a variety of spectroscopic methods and X-ray crystallography indicated that the reaction of iron(III) perchlorate, sodium hydroxide, and R_3TPA affords $[Fe_2(\mu\text{-}O)(\mu\text{-}OH)(R_3TPA)_2](ClO_4)_3$ (**2**) rather than the previously reported species $[Fe_2(\mu\text{-}O)(OH)(H_2O)(R_3TPA)_2](ClO_4)_3$ (**1**). Facile conversion of the (μ-oxo)(μ-hydroxo)diiron(III) core of **2** to the (μ-oxo)(hydroxo)(aqua)diiron(III) core of **1** occurs in the presence of water and at low temperature. When **2** is exposed to wet acetonitrile at room temperature, the CH_3CN adduct is hydrolyzed to CH_3COO^-, which forms the compound $[Fe_2(\mu\text{-}O)(\mu\text{-}CH_3COO)(R_3TPA)_2](ClO_4)_3$ (**10**). The identity of **10** was confirmed by comparison of its spectroscopic properties with those of an independently prepared sample. To evaluate whether or not **1** and **2** are capable of generating the diiron(IV) species $[Fe_2(\mu\text{-}O)(OH)(O)(R_3TPA)_2]^{3+}$ (**4**), which has previously been generated as a synthetic model for high-valent diiron protein oxygenated intermediates, studies were performed to investigate their reactivity with hydrogen peroxide. Because **2** reacts rapidly with hydrogen peroxide in CH_3CN but not in CH_3CN/H_2O, conditions that favor conversion to **1**, complex **1** is not a likely precursor to **4**. Compound **4** also forms in the reaction of **2** with H_2O_2 in solvents lacking a nitrile, suggesting that hydrolysis of CH_3CN is not involved in the H_2O_2 activation reaction. These findings shed light on the formation of several diiron complexes of electron-rich R_3TPA ligands and elaborate on conditions required to generate synthetic models of diiron(IV) protein intermediates with this ligand framework.

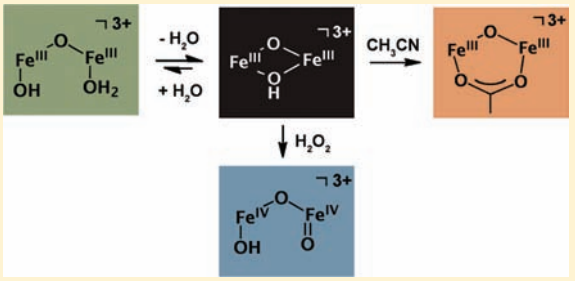

INTRODUCTION

Because of the importance of carboxylate-bridged diiron enzymes as powerful and selective oxidizing agents in bacterial systems such as soluble methane monooxygenase (sMMO),[1,2] understanding the chemical and physical characteristics of synthetic diiron(IV) units, which model the reactive species of the sMMO hydroxylase (sMMOH), is of considerable interest.[3−5] Among the various constructs employed to access such species, one convenient platform is based on a tripodal tris(pyridyl-2-methyl)amine (TPA) ligand. Stable dinuclear species can be readily prepared by linking two monomeric [Fe(TPA)] complexes through oxo, hydroxo, or carboxylato bridges.[6−8] A notable achievement in diiron TPA modeling chemistry is the crystallographic characterization of a mixed-valent di(μ-oxo)diiron(III,IV) unit, $[Fe_2(\mu\text{-}O)_2(5\text{-}Et_3\text{-}TPA)_2](ClO_4)_3$, where 5-$Et_3$-TPA = tris[(5-ethylpyridyl)-2-methyl]amine (Chart 1).[9,10] This complex contains the quadrilateral $\{Fe_2(\mu\text{-}O)_2\}$ core believed to be present in the diiron(IV) intermediate **Q** of sMMOH,[11] a remarkable enzyme that is capable of transforming methane to methanol.[12]

The electronic and steric properties of the diiron TPA complexes can be tuned by appending various substituents around the pyridine rings. Recently, studies using an electron-rich tris[(3,5-dimethyl-4-methoxy)pyridyl-2-methyl]amine (R_3TPA) derivative have enabled high-valent diiron units to be prepared.[13−15] Treatment of the diiron(III) precursor $[Fe_2(\mu\text{-}O)(OH)(H_2O)(R_3TPA)_2](ClO_4)_3$ (**1**, Chart 1) with H_2O_2 results in the formation of a di(μ-oxo)diiron(III,IV) $[Fe_2(\mu\text{-}O)_2(R_3TPA)_2]^{3+}$ (**7**) species.[13] When **7** was subjected to controlled bulk electrolysis at an applied potential of +900 mV (vs ferrocene/ferrocenium) in acetonitrile at −40 °C, a diiron(IV) $[Fe_2(\mu\text{-}O)_2(R_3TPA)_2]^{4+}$ (**5**) complex was quantitatively generated (Scheme 1). Compound **5** could also be accessed by chemical oxidation.[14] It was proposed that reaction of **1** with hydrogen peroxide and protons rapidly leads to formation of **5** through the transient generation of (μ-hydroperoxo)diiron(III,III) (**3**) and (μ-oxo)(hydroxo)(oxo)diiron(IV) (**4**) intermediates (Scheme 1). Compound **5**, however, exhibits poor hydrogen-atom abstraction

Received: November 2, 2011
Published: January 20, 2012

Chart 1. Depiction of $[Fe_2(\mu\text{-}O)_2(5\text{-Et-TPA})_2]^{3+}$ (left)[a] and $[Fe_2(\mu\text{-}O)(OH)(H_2O)(R_3TPA)_2]^{3+}$ (right)[b]

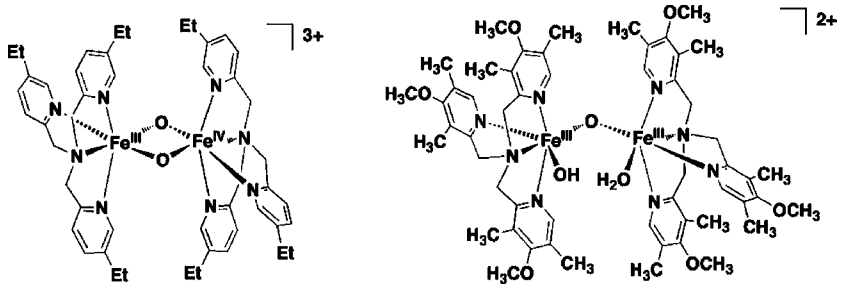

[a]The first di(μ-oxo)diiron(III,IV) species structurally characterized by X-ray crystallography. [b]This compound was reported to be a versatile starting material for generating diiron(IV) species. See reference 13.

Scheme 1. Reactions of a $[Fe^{III}_2(\mu\text{-}O)(\mu\text{-}OOH)(R_3TPA)_2]^{3+}$ (3) Species Leading to Formation of High-Valent Diiron(IV) and Diiron(III,IV) Units

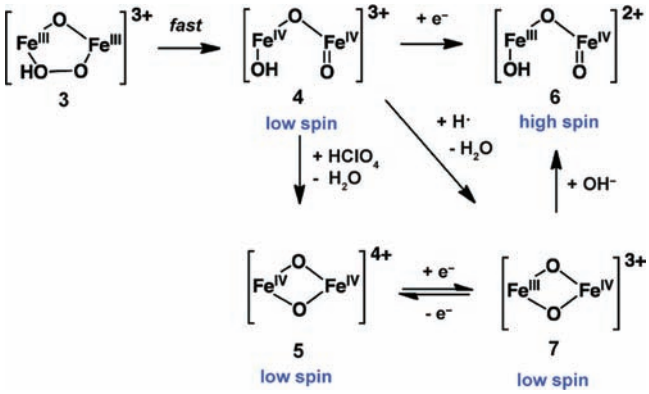

ability. When the valence-delocalized diiron(III,IV) **7** was treated with tetrabutylammonium hydroxide, or the diiron(IV) unit **4** was reduced by ferrocene, the valence-localized species **6** was obtained.[15] Compound **6** has a high-spin (S = 2) Fe^{IV}=O unit that displays a rate enhancement in hydrogen-atom abstraction reactions of several orders of magnitude compared to previously characterized high-valent diiron complexes with S = 1 Fe^{IV}=O units. In addition, conversion of the diamond core of **7** to a ring-opened structure by reaction with water or alcohol substrates also generates diiron species that are more reactive toward C−H bonds.[16]

During the course of extending these studies, we discovered that the reported procedure for preparing the starting material **1** produced the (μ-oxo)(μ-hydroxo)diiron(III) (**2**) species and an unidentified iron(III) side product. In this report, we describe the identity of **2** and provide an improved procedure for its preparation. The tendency of $\{Fe_2(\mu\text{-}O)_2\}$ units to undergo diiron core interconversion reactions in the presence of coordinating solvents was examined, which revealed that **2** can promote the hydrolysis of acetonitrile to form acetate. In light of these new findings, the reactivity of **2** with hydrogen peroxide was also more fully investigated. From these studies, we propose a revised reaction scheme for the generation of high-valent diiron units from diiron(III) R_3TPA precursors.

EXPERIMENTAL SECTION

Materials and Methods. Reagents obtained from commercial suppliers were used as received. Tris[(3,5-dimethyl-4-methoxypyridyl)-2-methyl]amine (R_3TPA) deuterated at the benzylic positions was prepared as previously described.[13] All manipulations were performed in air using standard laboratory techniques. Solvents were used as received from commercial suppliers without further purification.

General Physical Methods. NMR spectra were recorded at 500 MHz using Varian Mercury spectrometers; chemical shifts for ^{1}H and ^{13}C NMR spectra were referenced to residual solvent peaks. ^{1}H NMR spectral data of paramagnetic compounds were obtained by widening the sweep window (+100 to −30 ppm) and collecting for longer acquisition times (~1024 scans). IR spectra were recorded on a ThermoNicolet Avatar 360 spectrophotometer with the *OMNIC* software. Absorption spectra were recorded on a Cary 50 spectrophotometer using 6Q Spectrosil quartz cuvettes (Starna) with 1 cm path lengths. For low-temperature UV−vis measurements, a custom-made quartz cuvette (path length = 1.74 cm) containing a jacketed Dewar was employed. An acetonitrile/dry ice bath maintained the samples at −30 °C. Alternatively, absorption spectra and kinetic time traces at −40 °C were recorded on a Hewlett-Packard 8453A diode-array spectrometer equipped with a cryostat from Unisoku Scientific Instruments, Osaka, Japan. Mössbauer spectra were recorded on an MSI spectrometer (WEB Research Company) with a ^{57}Co source in a rhodium matrix at ambient temperature. Solid samples were prepared by suspension of the complex (~40 mg) in Apiezon M grease and placed in a nylon sample holder. Samples were measured over the course of ~5 days at 80 K. Isomer shift (δ) values are reported with respect to metallic iron used for velocity calibration at room temperature. Spectra were fit to Lorentzian lines using the *WMOSS* plot and fit program. Resonance Raman spectra were recorded on an Acton AM-506 spectrophotometer, using a Kaiser Optical holographic supernotch filter with a Princeton Instruments LN/CCD-1100-PB/UVAR detector cooled with liquid nitrogen. Laser excitation was provided by a Spectra Physics BeamLok 2060-RM argon-ion laser. The spectra were obtained at 77 K by using a 135° backscattering geometry, and the Raman frequencies were referenced to indene.

X-ray Data Collection and Refinement. Single crystals were mounted in Paratone oil using 30 μm aperture MiTeGen MicroMounts (Ithaca, NY) and frozen under a 100 K KRYO-FLEX nitrogen cold stream. Data were collected on a Bruker SMART APEX CCD X-ray diffractometer with Mo Kα radiation (λ = 0.710 73 Å) controlled by the *APEX 2* (version 2010.1-2) software package. Data reduction was performed using *SAINT*, and empirical absorption corrections were applied with *SADABS*.[17] The structures were solved by direct methods with refinement by full-matrix least squares based on F^2 using the *SHELXTL-97* software package[18] and checked for higher symmetry by the *PLATON* software.[19] All non-hydrogen atoms were located and refined anisotropically. Hydrogen atoms were fixed to idealized positions unless otherwise noted and given thermal parameters equal to either 1.5 (methyl hydrogen atoms) or 1.2 (non-methyl hydrogen atoms) times the thermal parameters of the atoms to which they are attached.

Complex **2** sits on an inversion center; thus, only half of the molecule is present in the asymmetric unit, along with 1.5 perchlorate anions and 2 acetonitrile molecules. Both perchlorate groups exhibit

dx.doi.org/10.1021/ic202379b | *Inorg. Chem.* 2012, 51, 2393−2402

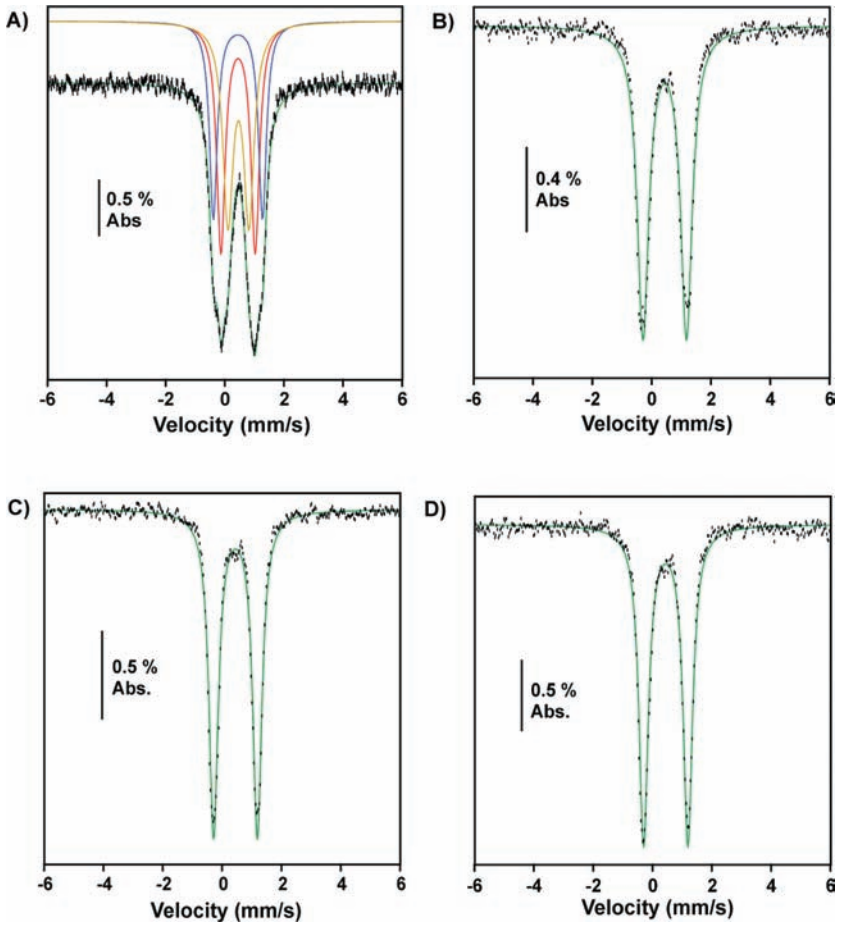

Figure 1. Zero-field Mössbauer spectra (80 K) of (A) crude material isolated from reaction of iron(III) perchlorate, sodium hydroxide, and R_3TPA; (B) compound **2**, (C) compound **10a**, and (D) compound **10b**. Spectrum A was best fit to three quadrupole doublets, whereas those of B, C, and D were adequately modeled with one-site fits. Raw data are in black, simulated fits are in green, and individual sites are in blue, yellow, and red.

positional disorder and were modeled accordingly. One of the ClO_4^- anions located on a special position was refined with 50% occupancy by suppressing generation of special position constraints. Due to charge considerations, the $\{Fe_2(\mu\text{-}O)_2\}$ core of **2** is best described as a (μ-oxo)(μ-hydroxo)diiron(III) unit, with the overall complex having the empirical formula $[Fe_2(\mu\text{-}O)(\mu\text{-}OH)(R_3TPA)_2](ClO_4)_3$. Thus, the observed Fe−O distances must result from disorder imposed by the symmetry of the unit cell averaged over Fe−O(oxo) and Fe−O(hydroxo) bond lengths. Although the core structures of **10a** and **10b** are identical, both containing the $[Fe_2(\mu\text{-}O)(\mu\text{-}CH_3CO_2)(R_3TPA)_2]^{3+}$ cation, they differ in the number of solvent molecules in their crystal lattices as well as their unit cell dimensions. The asymmetric unit of **10a** contains a single $[Fe_2(\mu\text{-}O)(\mu\text{-}CH_3CO_2)(R_3TPA)_2]^{3+}$ cation, together with three perchlorate anions and three acetonitrile moieties. Two of the ClO_4^- groups were modeled with positional disorder using appropriate similarity restraints and equal anisotropic displacement parameters. In contrast to **10a**, the asymmetric unit of **10b** has two independent molecules of $[Fe_2(\mu\text{-}O)(\mu\text{-}CH_3CO_2)(R_3TPA)_2](ClO_4)_3$, one diethyl ether, and five acetonitrile molecules. The diethyl ether unit is severely disordered, as is evident by the large anisotropic displacement parameters of its component atoms. Attempts to model this disorder did not give a stable refinement; thus, no attempt was made to do so in the final structure.

Kinetic Measurements. The rate of hydrolysis of acetonitrile by **2** was determined by UV−vis spectroscopic measurements. The data were recorded by scanning at 5 min intervals for 900 min. The absorption changes at 550 nm were fit to an A → B → C reaction sequence (eq 1), with rate constants k_1 and k_2, respectively. A simpler A → B kinetic model did not provide a satisfactory fit. The molar absorptivities ε_A, ε_B, and ε_C refer to species A, B, and C, respectively, and $[A]_0$ is the initial concentration of A.

$$\mathrm{Abs}_\lambda(t) = [A]_0 e^{-k_1 t}(\varepsilon_A - \varepsilon_C) + \frac{k_1}{k_2}[A]_0 \times (e^{-k_1 t} - e^{-k_2 t})(\varepsilon_B - \varepsilon_C) + [A]_0\varepsilon_C \quad (1)$$

Synthesis. *$[Fe_2(\mu\text{-}O)(\mu\text{-}OH)(R_3TPA)_2](ClO_4)_3$ (**2**).* Two methods, 1 and 2, give analytically pure **2**. *Method 1*: The published procedure for $[Fe_2(\mu\text{-}O)(OH)(H_2O)(R_3TPA)_2](ClO_4)_3$ (**1**),[13] which was mischaracterized in the original report, yields a crude solid that was extracted into dichloromethane and filtered to remove an insoluble impurity. The organic filtrate was evaporated to dryness to afford **2** as a red powder (114 mg, 42%). *Note: The aquated derivative of **2**, compound **1**, has not been isolated in the solid state but can be generated by treatment of **2** with excess water at low temperature.*

Method 2: R_3TPA (150 mg, 0.319 mmol) and $Fe(ClO_4)_3{\cdot}7.5H_2O$ (159 mg, 0.319 mmol; the number of water molecules was calculated based on the iron content stated on the Aldrich Certification of Analysis) were dissolved in 3 mL of MeOH. The resulting red solution was stirred at room temperature for 2 h. A 0.96 mL solution of a 500 mM NaOH stock solution in MeOH was added via a syringe pump over the course of 1 h. The solution was further stirred for 24 h, resulting in the precipitation of a red solid. About 3 mL of water was added in a dropwise manner, and the mixture was stirred for another 24 h. The pH of the solution was measured by a pH meter equipped with a glass electrode, giving a reading of ~5.5. The product was collected by filtration and washed with a 1:1 mixture of MeOH/H_2O. Yield: 231 mg, 75%. Red crystals suitable for X-ray crystallographic analysis were obtained by vapor diffusion of diethyl ether into an

dx.doi.org/10.1021/ic202379b | *Inorg. Chem.* 2012, 51, 2393−2402

Table 1. Summary of Spectroscopic Data

	crude solid					
	site 1	site 2	site 3	**2**	**10a**	**10b**
Mössbauer[a] δ (mm/s)	0.44	0.44	0.44	0.44	0.44	0.44
ΔE_Q (mm/s)	1.16	1.66	0.71	1.46	1.47	1.49
Γ (mm/s)	0.35	0.32	0.40	0.47	0.38	0.38
	36%	28%	36%			
UV–visible[b] λ_{max} (nm)	heterogeneous solution			370, 550	450, 490, 690	454, 504, 700
IR[c] ν (cm^{-1})	2945			2947	2927	2960
	1600			1599	1598	1599
	1575			1575	1576	1570
					1540	1532
	1478			1478	1478	1478
	1456			1455	1450	1450
	1401			1402	1402	1402
	1384			1384	1384	
	1293			1292	1292	1291
	1267			1268	1267	1264
	1077			1076	1091	1092
	1096					
	995			995	994	995
	874			874	875	875
				800 (w)		800
	768(w)			763(w)	765	764
	660			657(w)		
	623			624	623	623
^{1}H NMR[d] δ (ppm)	heterogeneous solution			4.70, 4.00, 3.89, 3.60, 3.42, 2.79, 2.24, 1.63	3.92, 3.68, 3.28, 2.94, 2.45	3.91, 3.67, 3.28, 2.93, 2.44

[a]Polycrystalline samples recorded at 80 K. [b]Recorded in dichloromethane at room temperature. [c]Measured as KBr pellets; IR peaks designated with a "w" indicate a weak intensity. [d]Recorded in chloroform-d_1.

acetonitrile solution of the compound. Crystals obtained from dichloromethane/diethyl ether were smaller than those grown from acetonitrile/diethyl ether. Note that hydrolysis of coordinated acetonitrile can occur to give $[Fe_2(\mu\text{-}O)(\mu\text{-}CH_3CO_2)(R_3TPA)_2](ClO_4)_3$; however, crystals of the acetate-bound diiron complex are yellow rather than red. Anal. Calcd for $[Fe_2(\mu\text{-}O)(\mu\text{-}OH)(R_3TPA)_2](ClO_4)_3 \cdot 4H_2O$ ($C_{54}H_{81}N_8Cl_3Fe_2O_{24}$): C, 44.91; H, 5.65; N, 7.76. Found: C, 45.24; H, 5.39; N, 7.85. ^{1}H NMR (CD_2Cl_2, 500 MHz): δ 4.70, 4.00, 3.89, 3.60, 3.42, 2.79, 2.24, 1.63. UV–vis (CH_2Cl_2): λ_{max} = 370, 550 nm. FT-IR (KBr): ν 2950, 2863, 1599, 1575, 1478, 1456, 1402, 1385, 1292, 1267, 1095, 1080, 997, 875, 800, 623 cm^{-1}. ^{57}Fe Mössbauer (80 K, apiezon grease): δ = 0.44(2) mm/s; ΔE_Q = 1.46(2) mm/s; $\Gamma_{L/R}$ = 0.47(2) mm/s. Mp (dec): 190 °C.

*$[Fe_2(\mu\text{-}O)(\mu\text{-}CH_3CO_2)(R_3TPA)_2](ClO_4)_3$ (**10b**).* Solid R_3TPA (200 mg, 426 μmol), $Fe(ClO_4)_3 \cdot 10H_2O$ (230 mg, 426 μmol), sodium acetate (17 mg, 213 μmol), and triethylamine (59 μL, 426 μmol) were dissolved in 2.0 mL of CH_3OH and stirred at room temperature for 3 h. A solid precipitate was isolated by filtration and washed with MeOH to afford a pale-yellow material (198 mg, 66%). Single crystals suitable for X-ray diffraction analysis were obtained from slow diffusion of diethyl ether into a solution of the compound in either acetonitrile or dichloromethane. ^{1}H NMR (CD_2Cl_2, 500 MHz): δ 3.91, 3.77, 3.67, 3.28, 2.92, 2.71, 2.44. UV–vis (CH_2Cl_2): λ_{max} = 332 (14 500 M^{-1} cm^{-1}), 374 (9850 M^{-1} cm^{-1}), 454 (1460 M^{-1} cm^{-1}), 504 (1,390 M^{-1} cm^{-1}), 700 (294 M^{-1} cm^{-1}) nm. FT-IR (KBr): ν 2960, 1599, 1532, 1478, 1402, 1264, 1092, 994, 875, 801, 764, 623 cm^{-1}. ^{57}Fe Mössbauer (80 K, apiezon grease): δ = 0.44(2) mm/s; ΔE_Q = 1.49(2) mm/s; $\Gamma_{L/R}$ = 0.38(2) mm/s. Anal. Calcd for $Fe_2C_{56}H_{75}N_8O_{21}Cl_3 \cdot CH_3OH$: C, 47.33; H, 5.51; N, 7.75. Found: C, 47.06; H, 5.32; N, 7.78. Mp (dec): 195 °C.

RESULTS AND DISCUSSION

Characterization of Diiron(III) Complexes of R_3TPA. Preparation of **1** was attempted according to the published procedure.[13] Reaction of iron(III) perchlorate decahydrate, R_3TPA, and sodium hydroxide in methanol and water afforded a red powder as described. However, it was discovered that this bulk material can be a heterogeneous mixture. Initially, this conclusion was derived from simple solubility tests, in which only some of the red solid could be extracted into common organic solvents, such as dichloromethane or acetonitrile. The fact that this crude compound was red, rather than green like other $[Fe_2(\mu\text{-}O)(OH)(H_2O)(L)_2]^{3+}$ compounds, where L = poly(N-donor) ligand, reported in the literature,[7,20,21] was also unexpected.

The zero-field ^{57}Fe Mössbauer spectrum of the crude red powder was best fit to three quadrupole doublets (Figure 1A), giving parameters δ_1 = 0.44 mm/s, ΔE_{Q1} = 1.16 mm/s, Area 1 = 36%; δ_2 = 0.44 mm/s, ΔE_{Q2} = 1.66 mm/s, Area 2 = 28%; and δ_3 = 0.44 mm/s, ΔE_{Q3} = 0.71 mm/s, Area 3 = 36% (Table 1). If the material contained pure **1**, two quadrupole doublets would be expected because each of the two iron atoms has a distinct coordination environment. This was indeed the case for $[Fe_2(\mu\text{-}O)(OH)(H_2O)(5\text{-}Me_3\text{-}TPA)_2]^{3+}$, which exhibited two quadrupole doublets of equal area.[9] The Mössbauer data for the crude red powder could then be interpreted as arising from at least two different complexes, accounting for the organic-soluble and -insoluble fractions. When the crude powder was extracted into dichloromethane, filtered, and evaporated to dryness, a slightly lighter red solid was obtained, hereafter referred to as compound **2**. As shown in Figure 1B, **2** exhibits a single quadrupole doublet having values of δ = 0.44 mm/s and ΔE_Q = 1.46 mm/s (Table 1). The Mössbauer parameters of **2** are most similar to those of site 2 in the crude material (method 1 in the Experimental Section), suggesting that the dichloromethane extraction and filtration steps facilitated purification of the product.

dx.doi.org/10.1021/ic202379b | Inorg. Chem. 2012, 51, 2393–2402

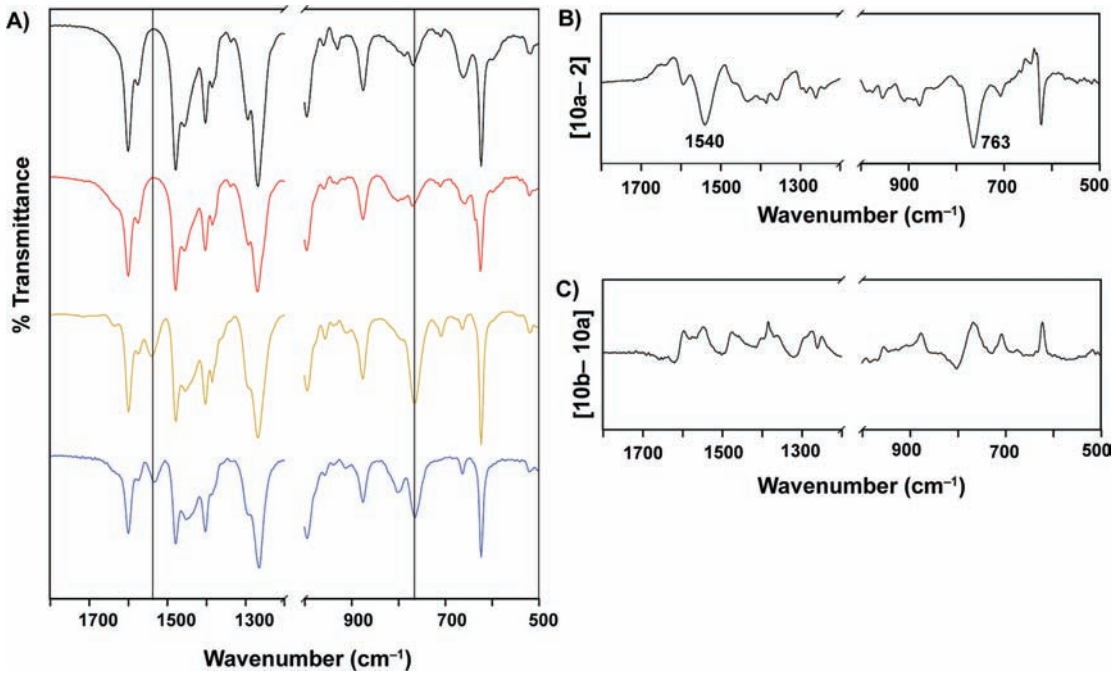

Figure 2. Stack plots of the FT-IR spectra (KBr pellets) of the crude material from reaction of iron(III) perchlorate, sodium hydroxide, and R_3TPA (black line), compound **2** (red line), compound **10a** (yellow line), and compound **10b** (blue line) (panel A). The difference spectra of **2**/**10a** (panel B) and **10a**/**10b** (panel C) are shown. The spectrum of **10a**, compared to that of **2**, displays two new peaks at 763 and 1540 cm^{-1}. No significant differences were observed in the spectrum of **10a** compared to that of **10b**. The spectral region from 1000 to 1200 cm^{-1} exhibits strong absorption from the perchlorate anion and has been omitted for clarity.

For a further comparison of the properties of the unpurified material to those of compound **2**, IR spectroscopy was employed. The IR spectra of the crude solid and **2** are shown in Figure 2A (black and red traces, respectively). As expected, both solids display intense bands at ~1100 cm^{-1}, characteristic of the perchlorate anion. The spectral envelope ranging from 500 to 1700 cm^{-1} is essentially identical for the two samples (Table 1), with some slight variations in weak baseline features. These data suggest that the insoluble fraction either has few IR-active features or has a composition similar to that of **2**.

In the course of our studies, we observed that the amount of insoluble material varied from batch to batch. We speculated that the amount of $Fe(ClO_4)_3$ in the reaction mixture and the addition rate of the NaOH solution might play important roles in determining the quality of complex **2** that was obtained. In particular, the amount of water in the hygroscopic $Fe(ClO_4)_3$ salt depended on the storage time and conditions and would therefore affect the actual amount of iron added to the reaction mixture. By using a $Fe(ClO_4)_3$ salt with a known amount of water and adding the NaOH solution slowly via a syringe pump (method 2 in the Experimental Section), we were able to reproducibly obtain samples of **2** containing a minimal amount of insoluble material.

Crystallization of **2** was attempted by slow diffusion of diethyl ether into a solution of the complex in acetonitrile. After several days, two different types of crystals were obtained, some red and others yellow. X-ray diffraction analysis of the red crystals revealed a diiron structure with an $\{Fe_2(\mu\text{-}O)_2\}$ core (Figure 3 and Table S1 in the Supporting Information). The iron atoms are separated by 2.79 Å and have pseudooctahedral coordination environments (Table 2). Each metal center is bound by a tetradentate R_3TPA ligand, with Fe−N(amine) and Fe−$N(pyridyl)_{ave}$ distances of 2.18 and 2.14 Å, respectively. Two oxygen atoms bridge the iron centers, with Fe−O bond

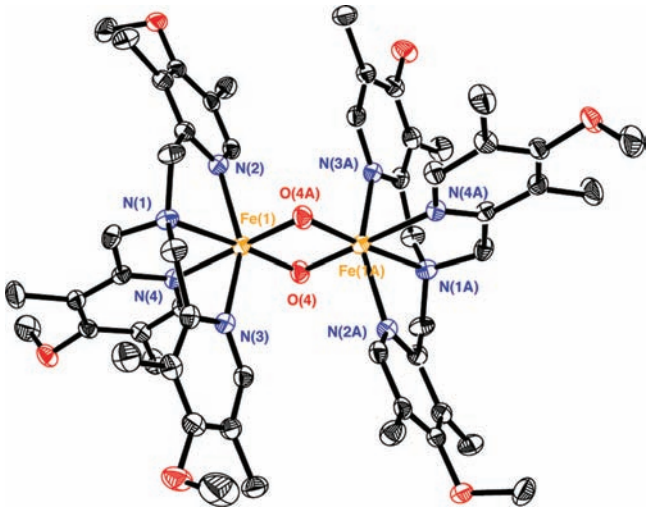

Figure 3. Thermal ellipsoid (50%) diagram of the X-ray structure of **2**. Hydrogen atoms, solvent molecules, and perchlorate anions are omitted for clarity. Color scheme: iron, orange; oxygen, red; nitrogen, blue; carbon, black. See Table S1 and Table 2 for the data refinement and structural parameters of **2**, respectively.

lengths of 1.88 and 1.93 Å. Because each diiron unit is associated with three perchlorate anions, charge-balance considerations indicate that the oxygen-atom bridges are best described as oxo and hydroxo ligands, giving the molecular formula $[Fe_2(\mu\text{-}O)(\mu\text{-}OH)(R_3TPA)_2](ClO_4)_3$. Because the molecule is located on an inversion center, the Fe−O bond types are disordered, with distances that are an average of iron−oxo and iron−hydroxo bond lengths. The structural parameters of **2** fall within the ranges exhibited by two isostructural diiron TPA complexes that differ only in their bridging oxygen-atom

dx.doi.org/10.1021/ic202379b | *Inorg. Chem.* 2012, 51, 2393−2402

Table 2. Selected Structural Parameters of 2, $[Fe_2(\mu\text{-}O)(\mu\text{-}OH)(6\text{-}Me_3TPA)_2](ClO_4)_3$, and $[Fe_2(\mu\text{-}O)_2(6\text{-}Me_3TPA)_2](ClO_4)_2$

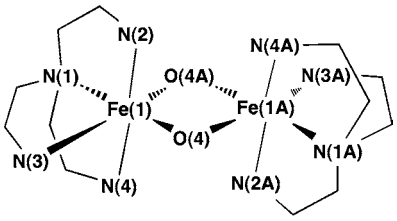

	2	$[Fe_2(\mu\text{-}O)(\mu\text{-}OH)(6\text{-}Me_3TPA)_2](ClO_4)_3$[b]	$[Fe_2(\mu\text{-}O)_2(6\text{-}Me_3TPA)_2](ClO_4)_2$[c]
Bond Distances (Å)[a]			
Fe(1)–Fe(1A)	2.7920(9)	2.95(1), 2.94(1)	2.716(2)
Fe(1)–O(4)	1.883(3)	1.906(8), 1.91(1)	1.844(3)
Fe(1)–O(4A)	1.934(2)	1.981(8), 1.960(9)	1.916(4)
Fe(1)–N(1)	2.183(3)	2.174(9), 2.18(1)	2.194(4)
Fe(1)–N(2)	2.147(3)	2.239(9), 2.28(1)	2.255(4)
Fe(1)–N(3)	2.151(3)	2.194(9), 2.196(9)	2.279(4)
Fe(1)–N(4)	2.134(3)	2.188(9), 2.18(1)	2.244(4)
Bond Angles (deg)[a]			
Fe(1)–O(4)–Fe(1A)	94.01(11)	98.7(4), 98.7(6)	92.5(2)
O(4)–Fe(1)–O(1A)	85.99(11)	81.3(4), 81.3(6)	87.5(2)
N(1)–Fe(1)–N(2)	76.24(10)	77.2(3), 76.0(5)	75.7(1)
N(1)–Fe(1)–N(3)	76.24(10)	81.2(4), 81.5(4)	74.7(2)
N(1)–Fe(1)–N(4)	79.74(10)	75.1(3), 75.6(4)	79.0(2)
N(1)–Fe(1)–O(4)	176.66(10)	170.6(4), 168.7(4)	175.1(2)
N(1)–Fe(1)–O(4A)	96.12(10)	89.4(4), 88.0(5)	87.8(2)

[a]A generalized numbering scheme, depicted in the above cartoon representation, is used. These atom labels do not necessarily correspond to those assigned in their respective X-ray structures. [b]Previously reported.[22] Each asymmetric unit contains two independent molecules. [c]Previously reported.[23]

protonation states, $[Fe_2(\mu\text{-}O)(\mu\text{-}OH)(6\text{-}Me_3TPA)_2](ClO_4)_3$[22] and $[Fe_2(\mu\text{-}O)_2(6\text{-}Me_3TPA)_2](ClO_4)_2$,[23] where 6-$Me_3$TPA = tris[(6-methylpyridyl)-2-methyl]amine (Table 2). On the basis of the similar spectroscopic properties of the red crystals compared to those of the red powder before crystallization, **2** is assigned as a (μ-oxo)(μ-hydroxo)diiron(III) complex. Related (oxo)diiron(III) complexes supported by TPA, 5-Me_3-TPA, and 5-Et_3-TPA ligands, previously synthesized using a procedure analogous to that of method 1 (see the Experimental Section),[9] are green in color, not red as observed for the R_3TPA complex. Because the visible bands of these complexes arise from transitions of the (μ-oxo)diiron(III) core, the difference in color most likely indicates a core structure having a different Fe–O–Fe angle.[6,8,9] Indeed, the X-ray crystal structure of a complex containing 5-Et_3-TPA has the $[Fe_2(\mu\text{-}O)(OH)(H_2O)(L)_2]^{3+}$ core with an Fe–O–Fe angle of 136°.[9] This result led some of us to assume, incorrectly, that the same core structure would be obtained in the case of R_3TPA.[13] The R_3TPA ligand has one methoxy and two methyl substituents on each pyridine donor, compared to TPA, 5-Me_3-TPA, and 5-Et_3-TPA, which have at most one electron-donating substituent on each pyridine ring. We conjecture that the more electron-donating nature of R_3TPA stabilizes the $[Fe_2(\mu\text{-}O)(\mu\text{-}OH)]$ core of **2**, allowing it to be crystallized.

The yellow crystals, which were obtained unexpectedly from crystallization of **2** in acetonitrile/diethyl ether, were also evaluated by X-ray crystallography (Figure 4 and Table S1). The compound has a dinuclear structure with an Fe–Fe distance of 3.25 Å (Table S2). Each pseudooctahedral iron atom is capped by a R_3TPA group, with $Fe–N(amine)_{ave}$ = 2.20 Å and $Fe–N(pyridyl)_{ave}$ = 2.15 Å, and is linked by two bridging ligands. One of the bridges is an oxo anion, as indicated by

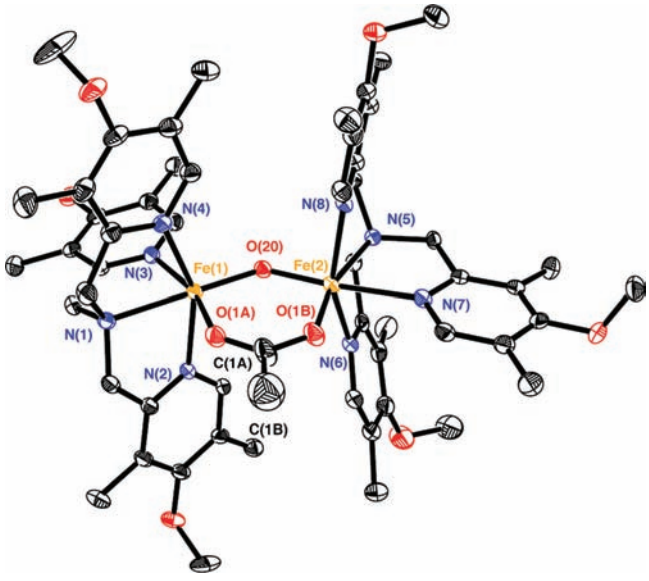

Figure 4. Thermal ellipsoid (50%) diagram of the X-ray structure of $[Fe_2(\mu\text{-}O)(\mu\text{-}CH_3CO_2)(R_3TPA)_2](ClO_4)_3{\cdot}2CH_3CN$ (**10a**). Hydrogen atoms, solvent molecules, and perchlorate anions are omitted for clarity. Color scheme: iron, orange; oxygen, red; nitrogen, blue; carbon, black. See Tables S1 and S2 for the data refinement and structural parameters of **10a**, respectively.

short Fe–O bond lengths of ~1.80 Å. A difference electron density map revealed that the second bridging ligand contains four non-hydrogen atoms arranged in a trigonal-planar geometry. Assigning this group to an acetate moiety allowed the structure to refine to convergence, with Fe–O distances of 2.04 and 1.96 Å. The presence of an acetate moiety in this structure

dx.doi.org/10.1021/ic202379b | Inorg. Chem. 2012, 51, 2393–2402

is surprising because no such anion was present during the preparation or crystallization of **2**. Because there are three perchlorate anions for each diiron unit, we assign the molecular formula as $[Fe_2(\mu\text{-}O)(\mu\text{-}CH_3CO_2)(R_3TPA)_2](ClO_4)_3$ (**10a**). These results indicate that, although compound **2** is readily prepared in pure form, when dissolved in acetonitrile, **10a** can form.

As expected, compounds **2** and **10a** display distinctive optical spectra (Figure S1). The absorption spectrum of **2** has λ_{max} values at 370 and 550 nm, which are characteristic of (μ-oxo)(μ-hydroxo)diiron(III) rather than di(μ-oxo)diiron(III) species.[8] The visible band at 550 nm has been attributed to an oxo-to-iron(III) charge transfer. In contrast, **10a** exhibits optical bands at 332, 454, 492, and 700 nm. These features are identical with those reported for other (μ-oxo)(μ-carboxylato)-diiron(III) TPA species.[6]

The IR spectra of the red and yellow crystals of **2** and **10a**, respectively, were recorded (Figure 2A). Because of similarities in their molecular composition, **2** and **10a** share several prominent features in the spectral range between 500 and 1700 cm^{-1}. In addition to the vibrational modes present in the spectrum of **2**, however, **10a** displays peaks at 763 and 1540 cm^{-1} (Figure 2B). The former is ascribed to an asymmetric Fe−O−Fe stretching mode and the latter to an asymmetric C−O−O^- vibration of the bridging acetate. From several comprehensive studies of synthetic oxo-bridged diiron(III) compounds,[24,25] it has been established that the Fe−O stretching frequency of an $\{Fe_2(\mu\text{-}O)\}^{4+}$ unit is strongly correlated with its Fe−O−Fe angle. Because the Fe−O−Fe angle in **2** (94°) is significantly smaller than that of **10a** (130°), the ν_{Fe-O} stretching frequencies of **2** are expected to occur at higher energies than those in **10a**. Without further ^{18}O isotopic labeling studies, however, the Fe−O mode of **2** cannot be definitively assigned. Nevertheless, the IR data clearly show that **10a** contains a carboxylate group, whereas **2** does not. These results are consistent with the formulation of **2** as $[Fe_2(\mu\text{-}O)(\mu\text{-}OH)(R_3TPA)_2](ClO_4)_3$ and **10a** as $[Fe_2(\mu\text{-}O)(\mu\text{-}CH_3CO_2)(R_3TPA)_2](ClO_4)_3$.

The ^1H NMR spectra of **2** and **10a** are indicative of paramagnetic species at room temperature. The spectrum of **2** shows several significantly broadened peaks at δ 4.70, 4.00, 3.89, 3.60, 3.42, 2.79, 2.24, and 1.63 (Figure 5A), whereas those for **10a** appear at δ 3.92, 3.68, 3.28, 2.94, and 2.45 (Figure 5B). Previous studies of iron TPA complexes have indicated that the β protons of its pyridine rings are highly sensitive to the electronic properties of the iron centers; no attempt was made to examine this property in the present work.[8]

To further confirm the identity of complex **10a**, particularly the assignment of acetate as its bridging ligand, efforts were made to prepare $[Fe_2(\mu\text{-}O)(\mu\text{-}CH_3CO_2)(R_3TPA)_2](ClO_4)_3$ independently. Reaction of solid R_3TPA, iron(III) perchlorate decahydrate, sodium acetate, and triethylamine in a 2:2:1:2 ratio in a methanol solution afforded a yellow precipitate that was readily isolated by filtration. Single crystals of the compound were obtained by slow diffusion of diethyl ether into an acetonitrile solution. X-ray diffraction analysis of these yellow blocks showed two molecules of $[Fe_2(\mu\text{-}O)(\mu\text{-}CH_3CO_2)(R_3TPA)_2]^{3+}$ in the asymmetric unit (Figure S2), along with six perchlorate anions, five acetonitrile molecules, and one diethyl ether. The $[Fe_2(\mu\text{-}O)(\mu\text{-}CH_3CO_2)(R_3TPA)_2](ClO_4)_3$ compound obtained from this preparation will hereafter be referred to as **10b**. Table S2 lists the metrical parameters of the structures of **10a** and **10b**. The two structures have essentially identical bond distances and angles, with deviations

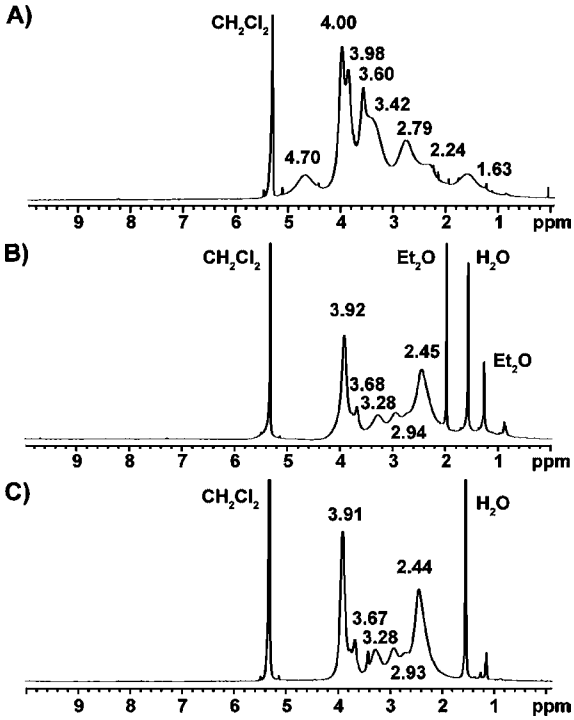

Figure 5. ^1H NMR spectra (CD_2Cl_2, 500 MHz) of (A) complex **2**, (B) complex **10a**, and (C) complex **10b** recorded at room temperature.

that are no greater than ~0.01 Å or ~1°, respectively. The small structural differences between **10a** and **10b** can be accounted for by crystal packing, for the two unit cells have different dimensions as a result of different numbers of solvent molecules in their lattices (Table S1). For discussion purposes, if the origin of the $[Fe_2(\mu\text{-}O)(\mu\text{-}CH_3CO_2)(R_3TPA)_2](ClO_4)_3$ complex is unimportant, we hereafter refer to the compound as **10**, without an "**a**" or "**b**" annotation.

To obtain further evidence that **10a** and **10b** are indeed the same compound, ^{57}Fe Mössbauer spectra were recorded. Both display a single quadrupole doublet. The data for **10a** were fit with δ = 0.44 mm/s and ΔE_Q = 1.47 mm/s, whereas those for **10b** were fit with δ = 0.44 mm/s and ΔE_Q = 1.49 mm/s (Table 1). Although the two iron atoms in $[Fe_2(\mu\text{-}O)(\mu\text{-}CH_3CO_2)(R_3TPA)_2](ClO_4)_3$ are not related by molecular symmetry, the similarity in their coordination environments makes them indistinguishable by zero-field Mössbauer spectroscopy. These Mössbauer parameters are typical for iron in the 3+ oxidation state and compare favorably with those of other (μ-oxo)(μ-carboxylato)diiron(III) TPA compounds.[6]

Finally, the UV−vis (Figure S1, blue) and ^1H NMR spectra of **10b** (Figure 5C) are identical with those of **10a** (Figure S1, yellow, and Figure 5B, respectively). In summary, the evidence is unequivocal that the four-atom bridging ligand in **10a** is acetate.

Effect of Solvent, Temperature, and Water on the Stability of 2. To examine the stability of the (μ-oxo)(μ-hydroxo)diiron(III) core of **2** in solution, its absorption spectrum was recorded in different solvents at room temperature (Figure S3). The oxo-to-iron(III) charge-transfer band at 550 nm is present when **2** is dissolved in either neat dichloromethane or acetonitrile. Dissolution of **2** in an equal mixture of dichloromethane and methanol, however, led to complete loss of this optical feature. The disappearance of the 550 nm band indicates that there is a change in the diiron core, perhaps resulting from

dx.doi.org/10.1021/ic202379b | Inorg. Chem. 2012, 51, 2393−2402

a loss of one of the bridging ligands, conversion of the hydroxide to a methoxide bridge, or dissociation into mononuclear iron species. Although this behavior was observed only when methanol was introduced into dichloromethane, other protic solvents may have similar effects on **2**.

It has been documented that the (μ-oxo)(μ-hydroxo)-diiron(III) core can convert to a (μ-oxo)(hydroxo)(aqua)diiron(III) unit through a temperature-dependent aquation reaction.[8,21] When a solution of **2** in acetonitrile was cooled to −30 °C under ambient conditions, the prominent band at 550 nm decreased in intensity (Figure S4, red trace) and disappeared completely upon treatment with ∼8000 equiv of H_2O (green trace). When the solution was warmed to room temperature, the 550 nm band of **2** was partially restored (blue trace). It is likely that, upon cooling of **2** in solution, partial aquation from trace water in the solvent occurs to afford **1**. When H_2O was deliberately added to the solution at −30 °C, **2** was completely converted to **1**. This equilibrium shifted back predominantly toward **2** when the solution was warmed to room temperature.

To obtain a quantitative measure of the affinity of **2** for H_2O at low temperature, the equilibrium constant for conversion between **1** and **2** was determined. As shown in Figure 6, titrat-

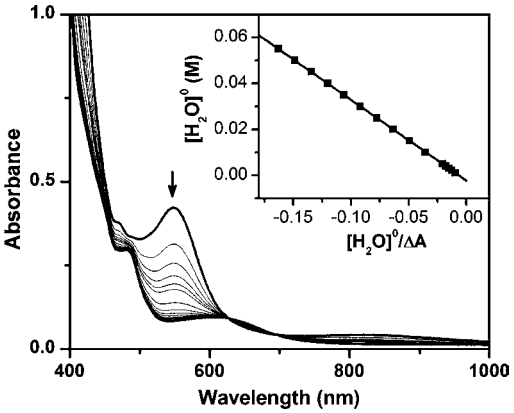

Figure 6. UV−vis spectra of a 0.5 mM solution of complex **2** in CH_3CN at −40 °C upon titration with water. Inset: plot of $[H_2O]^0$ (total added water concentration) versus $[H_2O]^0/\Delta A$ (absorbance change at 550 nm), from which a dissociation constant of water (K_d) in the hydrated form of **2** (complex **1**) is determined to be 0.0022(1) M. Upon addition of 50 mM H_2O, [**1**]/[**2**] = $[H_2O]/K_d$ = 22, meaning that over 95% of the iron complex is in the hydrated form. The K_d value was determined from these optical data using a model described previously.[29]

ion of water to a solution of **2** resulted in disappearance of the 550 nm absorbance, indicating formation of **1**. From these data, a dissociation constant (K_d) of 0.0022(1) M was determined for the reaction shown in eq 2.

$$[Fe_2(\mu\text{-}O)(OH)(H_2O)(R_3TPA)_2]^{3+}\ (\mathbf{1}) \rightleftharpoons [Fe_2(\mu\text{-}O)(\mu\text{-}OH)(R_3TPA)_2]^{3+}\ (\mathbf{2}) + H_2O \quad (2)$$

This K_d value indicates that, for a 0.5 mM solution of **2**, having a water concentration of 50 mM would convert **2** to greater than 95% of the hydrated complex **1** at −40 °C.

We also carried out resonance Raman experiments in an attempt to find support for the conclusion from UV−vis spectroscopy that **2** converts to **1** in an acetonitrile solution. Unfortunately, we were unsuccessful in obtaining a Raman spectrum of **2** in the solid state or in a frozen dichloromethane solution, conditions under which the characteristic red color of the $\{Fe_2(\mu\text{-}O)(\mu\text{-}OH)\}^{3+}$ core is retained. On the other hand, a Raman spectrum could be observed in a frozen acetonitrile solution. Upon freezing, however, the color of the solution turned from red to green, suggesting conversion of **2** to **1**. The coordinated water molecule in **1** formed in such a manner would have to derive from water trapped in the solid-state lattice of **2**, which was precipitated from CH_3OH/H_2O during its preparation. Upon 457.9 nm excitation, two prominent resonance-enhanced peaks appeared at 457 and 770 cm^{-1} (Figure 7). These features are assigned respectively to the

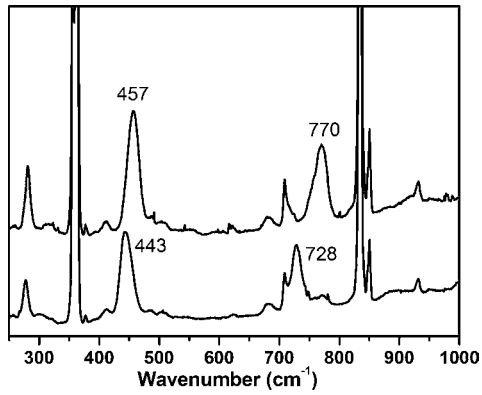

Figure 7. Raman spectra of 10 mM ^{16}O- (top) and ^{18}O-labeled (bottom) **2** in frozen CH_3CN-d_3 (77 K). Excitation: 457.9 nm. The peaks at 457 and 770 cm^{-1} arise from the symmetric and asymmetric vibration modes of the Fe−O−Fe unit, respectively.

symmetric and asymmetric vibrational modes of the Fe−O−Fe moiety and exhibit the expected isotopic shifts upon ^{18}O labeling. On the basis of extensive studies of similar oxo-bridged diiron units,[8] these $\nu_{Fe-O-Fe}$ values correspond to an Fe−O−Fe angle within the range of 130−143°, consistent with the Fe−O−Fe angle of 136° found in the X-ray structure of the (μ-oxo)(hydroxo)(aqua)diiron(III) complex supported by the 5-Et_3-TPA ligand.[9] On the other hand, the (μ-oxo)(μ-hydroxo)diiron(III) core of **2** with an Fe−O−Fe angle of 94° (Table 2) would have been predicted to exhibit Raman bands at ca. 600 and 670 cm^{-1}, by analogy to the bands observed for $[Fe^{III}_2(\mu\text{-}O)(\mu\text{-}OH)(6\text{-}Me_3TPA)_2]^{3+}$ and $[Fe^{III}_2(\mu\text{-}O)_2(6\text{-}Me_3TPA)_2]^{2+}$, which have Fe−O−Fe angles of 98.7° and 92.5°, respectively.[8]

Hydrolysis of Acetonitrile to Acetate. The yellow crystals of **10a** isolated from crystallization of **2** in acetonitrile could result either from a contaminant or through a chemical process that converts **2** to **10** under the conditions employed. Because no sources of acetate were used during the preparation of **2** and the results were verified by multiple independent experiments, the latter is more likely. Dimetallic complexes are known to promote the hydrolysis of organonitriles.[26−28] As depicted in Scheme 2, it is possible that even at room temperature trace amounts of water in the solvent react with **2** to give **1**. A CH_3CN molecule can then displace the coordinated water in **1** to give the acetonitrile adduct **8**. In the first irreversible step, the hydroxide ligand bound to the other iron atom in **1** attacks the electrophilic nitrile group, affording a (μ-oxo)(μ-acetamido)diiron(III) species **9**. For most nitrogen-rich diiron compounds, the hydrolysis of CH_3CN does not proceed beyond the carboxamide.[7,20] Because **10**, rather than **9**,

dx.doi.org/10.1021/ic202379b | Inorg. Chem. 2012, 51, 2393−2402

Scheme 2. Proposed Pathway for the Complete Hydrolysis of Acetonitrile to Acetate Mediated by a $[Fe_2(\mu\text{-}O)(\mu\text{-}OH)(R_3TPA)_2]^{3+}$ (2) Complex

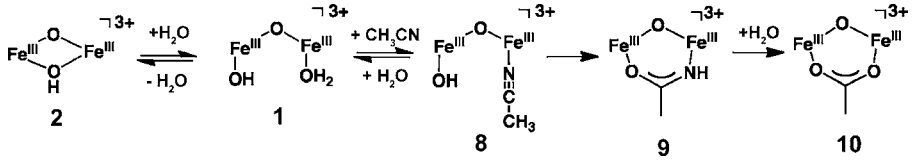

was isolated from the crystallization of **2**, hydrolysis of the acetamide in **9** must occur to afford the acetate.

To obtain evidence for the complete hydrolysis of CH_3CN, the absorption spectrum of **2** in acetonitrile was recorded over the course of ~900 min. The reaction was performed with wet solvent in air at room temperature to reproduce the conditions under which **10a** was crystallized. Although the reaction is slow, spectral changes were observed between 340 and 380 nm as well as at 550 nm (Figure S5A). The kinetic data at 553 nm were fit satisfactorily to a two consecutive unimolecular reaction model, yielding rate constants of $k_1 = 2.04 \pm 0.16 \times 10^{-2}$ min^{-1} and $k_2 = 1.98 \pm 0.06 \times 10^{-3}$ min^{-1} (Figure S5B). These processes are tentatively attributed to conversion of **2** to **9** and of **9** to **10** (Scheme 2). A (μ-oxo)(μ-acetamido)-diiron(III) complex **9** has not been isolated from the reaction mixture but is a logical precursor to **10**.

Reaction of 2 with Hydrogen Peroxide. Because the diiron(III) R_3TPA complex can exist in two forms in solution, either as a (μ-oxo)(μ-hydroxo)diiron(III) (**2**) or a (μ-oxo)-(hydroxo)(aqua)diiron(III) (**1**) species, it was of interest to determine whether both units are capable of generating the same high-valent diiron intermediates. When **2** was treated with H_2O_2 in anhydrous acetonitrile at −40 °C, its absorption spectrum displayed a broad feature centered at ~705 nm (Figure 8). As previously reported,[14] this spectrum corresponds

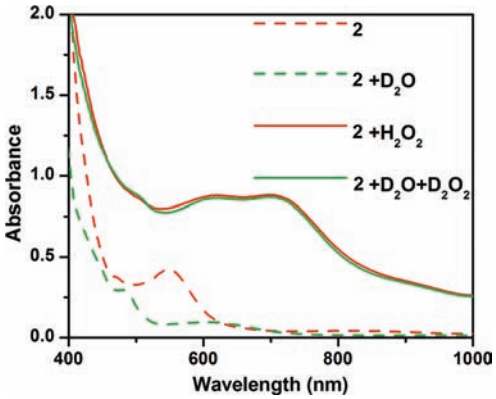

Figure 8. UV−vis spectra of 0.5 mM **2** in anhydrous CH_3CN (red dashed line) and after reaction with 0.5 mM H_2O_2 (red solid line), as well as 0.5 mM **2** in CH_3CN with 50 mM D_2O (green dashed line) and after reaction with 0.5 mM D_2O_2 (green solid line). All spectra were measured at −40 °C. These data show that both **1** and **2** react with H_2O_2 to generate the $[HO{-}Fe^{IV}{-}O{-}Fe^{IV}{=}O]^{3+}$ (**4**) product in the same yield (~70% with respect to **2**).

to the diiron(IV) complex $[Fe^{IV}_2(\mu\text{-}O)(OH)(O)(R_3TPA)_2]^{3+}$ (**4**) (Scheme 1). When **2** was treated with H_2O_2 in the presence of 50 mM H_2O, which essentially converts **2** to **1**, significantly greater amounts of the $[Fe^{III}Fe^{IV}(\mu\text{-}O)_2(R_3TPA)_2]^{3+}$ (**7**; λ_{max} = 620 nm) side product were observed (Figure S6). Addition of deuterated D_2O_2/D_2O instead of H_2O_2/H_2O, however, afforded a greater yield of **4** (Figure 8). Although both complexes **1** and **2** yield **4** upon exposure to hydrogen peroxide, they react at significantly different rates. As shown by the time trace in Figure 9, when **2** was treated with H_2O_2 in a dry

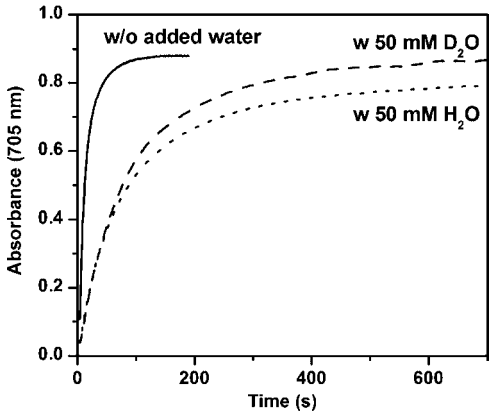

Figure 9. Time traces showing different rates for reactions of **2** with hydrogen peroxide in the absence (solid line) or presence of 50 mM added water [H_2O_2/H_2O (dotted line) or D_2O_2/D_2O (dashed line)] in CH_3CN at −40 °C.

solvent at −40 °C, the reaction was complete in less than 100 s. In contrast, when the reaction was performed in the presence of 50 mM water, it took approximately 600 s to obtain the maximum yield of **4**. This result strongly suggests that hydrogen peroxide reacts directly with **2** but not **1** and that water inhibits the formation of **4** by driving the solution equilibrium toward **1** (Scheme 3).

To eliminate the possible reaction of **2** with acetonitrile to afford the (μ-oxo)(μ-acetato)diiron(III) complex **10** in the course of H_2O_2 activation, the reaction of **2** with hydrogen peroxide was examined in other solvents. As indicated by the lack of an absorption band at 550 nm when **2** was dissolved in commercial-grade acetone (Figure S7, dotted line), the complex was fully transformed to **1**, presumably because of the high content of water in the solvent. Because H_2O competes with H_2O_2 for reaction with **2**, the solution was treated with 2 equiv of H_2O_2, instead of 1 equiv, to favor the formation of high-valent diiron species (Figure S7). After ~30 s, the absorption spectrum showed a feature at 705 nm, corresponding to **4**. After ~1000 s, a prominent band at 620 nm had fully developed, indicating that the mixed-valent diiron(III,IV) species **7** is the final product. When **2** was dissolved in a CH_2Cl_2/CH_3CN (3:1) mixture, the (μ-oxo)(μ-hydroxo)-diiron(III) core of **2** remained intact (Figure S8). Upon treatment with 1 equiv of H_2O_2, **2** had converted mostly to **4**, together with a small amount of **7**. Although formation of **4** from **2**/H_2O_2 occurs most cleanly in anhydrous acetonitrile, the fact that it also forms in solvents other than CH_3CN demonstrates

dx.doi.org/10.1021/ic202379b | Inorg. Chem. 2012, 51, 2393−2402

Scheme 3. Hydrogen Peroxide Reacts Directly with 2, Not 1[a]

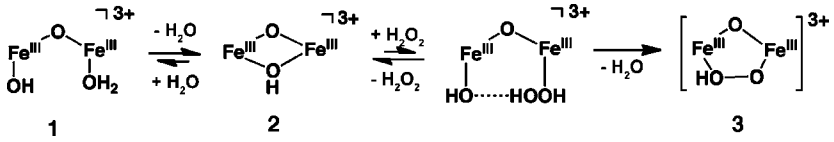

[a]This scheme is revised from that previously reported.

that acetonitrile hydrolysis is not involved in H_2O_2 activation by **2**.

CONCLUSION

Through a combination of spectroscopic and crystallographic investigations, the diiron(III) complex prepared from iron(III) perchlorate, sodium hydroxide, and R_3TPA was determined to have the composition $[Fe_2(\mu\text{-}O)(\mu\text{-}OH)(R_3TPA)_2](ClO_4)_3$ (**2**) rather than **1**. Conversion of **2** to **1** is favored in the presence of water and at low temperature in solution. To date, compound **1** has not been isolated in pure form in the solid state. Prolonged dissolution of **2** in wet acetonitrile at room temperature led to complete hydrolysis of the nitrile group of CH_3CN to CH_3COO^-. This transformation is unusual in that similar reactions mediated by iron(III) complexes do not typically proceed beyond the formation of acetamide.[7,20] Further reactivity studies demonstrate that the (μ-oxo)(μ-hydroxo)diiron(III) core of **2** reacts readily with H_2O_2 but that the (μ-oxo)(hydroxo)(aqua)diiron(III) core of **1** does not. In fact, the addition of water to **2** retards the formation rate of high-valent diiron intermediates, suggesting that **1** does not lie along the reaction pathway to complex **4**. Activation of hydrogen peroxide by **2** also occurs in non-nitrile-containing solvents, although the yield of **4** is much lower than when the reaction is performed in acetonitrile. This work has led to a better understanding of the nature of the diiron species supported by the electron-rich R_3TPA ligand and the requirements for generating high-valent diiron(IV) complexes of possible relevance to carboxylate-bridged diiron enzymes that activate dioxygen.

ASSOCIATED CONTENT

Supporting Information

X-ray crystallographic data in CIF format and table, structural comparison table, and UV−vis absorption data. This material is available free of charge via the Internet at http://pubs.acs.org.

AUTHOR INFORMATION

Corresponding Author

*E-mail: lippard@mit.edu (S.J.L.), larryque@umn.edu (L.Q.).

ACKNOWLEDGMENTS

The authors thank the National Institute of General Medical Sciences (Grant GM-032134 to S.J.L. and Grant GM-38767 to L.Q.) for supporting this work.

REFERENCES

(1) Feig, A. L.; Lippard, S. J. *Chem. Rev.* **1994**, *94*, 759−805.
(2) Wallar, B. J.; Lipscomb, J. D. *Chem. Rev.* **1996**, *96*, 2625−2658.
(3) Du Bois, J.; Mizoguchi, T. J.; Lippard, S. J. *Coord. Chem. Rev.* **2000**, *200−202*, 443−485.
(4) Que, L. Jr.; Tolman, W. B. *Nature* **2008**, *455*, 333−340.
(5) Friedle, S.; Reisner, E.; Lippard, S. J. *Chem. Soc. Rev.* **2010**, *39*, 2768−2779.
(6) Norman, R. E.; Yan, S.; Que, L. Jr.; Backes, G.; Ling, J.; Sanders-Loehr, J.; Zhang, J. H.; O'Connor, C. J. *J. Am. Chem. Soc.* **1990**, *112*, 1554−1562.
(7) Hazell, A.; Jensen, K. B.; McKenzie, C. J.; Toftlund, H. *Inorg. Chem.* **1994**, *33*, 3127−3134.
(8) Zheng, H.; Zang, Y.; Dong, Y.; Young, V. G. Jr.; Que, L. Jr. *J. Am. Chem. Soc.* **1999**, *121*, 2226−2235.
(9) Dong, Y.; Fujii, H.; Hendrich, M. P.; Leising, R. A.; Pan, G.; Randall, C. R.; Wilkinson, E. C.; Zang, Y.; Que, L. Jr.; Fox, B. G.; Kauffmann, K.; Münck, E. *J. Am. Chem. Soc.* **1995**, *117*, 2778−2792.
(10) Hsu, H.-F.; Dong, Y.; Shu, L.; Young, V. G. Jr.; Que, L. Jr. *J. Am. Chem. Soc.* **1999**, *121*, 5230−5237.
(11) Shu, L.; Nesheim, J. C.; Kauffmann, K.; Münck, E.; Lipscomb, J. D.; Que, L. Jr. *Science* **1997**, *275*, 515−518.
(12) Tinberg, C. E.; Lippard, S. J. *Acc. Chem. Res.* **2011**, *44*, 280−288.
(13) Xue, G.; Wang, D.; De Hont, R.; Fiedler, A. T.; Shan, X.; Münck, E.; Que, L. Jr. *Proc. Natl. Acad. Sci. U.S.A.* **2007**, *104*, 20713−20718.
(14) Xue, G.; Fiedler, A. T.; Martinho, M.; Münck, E.; Que, L. Jr. *Proc. Natl. Acad. Sci. U.S.A.* **2008**, *105*, 20615−20620.
(15) Xue, G.; De Hont, R.; Münck, E.; Que, L. Jr. *Nat. Chem.* **2010**, *2*, 400−405.
(16) Xue, G.; Pokutsa, A.; Que, L. Jr. *J. Am. Chem. Soc.* **2011**, *133*, 16657−16667.
(17) Sheldrick, G. M. *SADABS: Area Detector Absorption Correction*; University of Göttingen: Göttingen, Germany, 2001.
(18) Sheldrick, G. M. *Acta Crystallogr., Sect. A* **2008**, *A64*, 112−122.
(19) Spek, A. L. *PLATON, A Mutipurpose Crystallographic Tool*; Utrecht University, Utrecht, The Netherlands, 2000.
(20) Wilkinson, E. C.; Dong, Y.; Que, L. Jr. *J. Am. Chem. Soc.* **1994**, *116*, 8394−8395.
(21) Poussereau, S.; Blondin, G.; Cesario, M.; Guilhem, J.; Chottard, G.; Gonnet, F.; Girerd, J.-J. *Inorg. Chem.* **1998**, *37*, 3127−3132.
(22) Zang, Y.; Pan, G.; Que, L. Jr.; Fox, B. G.; Münck, E. *J. Am. Chem. Soc.* **1994**, *116*, 3653−3654.
(23) Zang, Y.; Dong, Y.; Que, L. Jr.; Kauffmann, K.; Münck, E. *J. Am. Chem. Soc.* **1995**, *117*, 1169−1170.
(24) Sanders-Loehr, J.; Wheeler, W. D.; Shiemke, A. K.; Averill, B. A.; Loehr, T. M. *J. Am. Chem. Soc.* **1989**, *111*, 8084−8093.
(25) Kurtz, D. M. Jr. *Chem. Rev.* **1990**, *90*, 585−606.
(26) Curtis, N. J.; Hagen, K. S.; Sargeson, A. M. *J. Chem. Soc., Chem. Commun.* **1984**, 1571−1573.
(27) Kukushkin, V. Y.; Pombeiro, A. J. L. *Chem. Rev.* **2002**, *102*, 1771−1802.
(28) Borriello, C.; Centore, R.; Roviello, G. *Inorg. Chem. Commun.* **2005**, *8*, 755−758.
(29) Praneeth, V. K. K.; Näther, C.; Peters, G.; Lehnert, N. *Inorg. Chem.* **2006**, *45*, 2795−2811.